




Bilayered nanosheets used for complex topography wound anti-infection

Chengkai Xuan^{2,3,4} · Xuemin Liu^{2,3,4} · Chen Lai¹ · Xuetao Shi^{1,2,3,4} 

Received: 26 May 2020 / Accepted: 1 August 2020 / Published online: 20 August 2020
© Zhejiang University Press 2020

Abstract

There is a consensus that the prevention of wound infection should be achieved in the following ways: (1) closing the wound to protect it from extra infection; (2) an antibacterial agent that could kill endogenous bacteria. However, existing bulk two-dimensional antibacterial materials show inefficient adhesion to wounds with complex morphology and thus cause the prevention of wound closure. Reducing the thickness of bulk two-dimensional materials to less than 100 nanometres endows them with great flexibility, which could allow them to adhere to wounds with complex morphology by only physical adhesion. Herein, a broad-spectrum and efficient antimicrobial peptide (AMP) was introduced to biocompatible methacrylated gelatine (GelMA) with multiple modification sites, which served as an inner antibacterial layer. After being combined with a biodegradable and good mechanical poly-L-lactide (PLLA) outer layer through plasma-treatment-assisted spin coating, we finally constructed bilayered antibacterial nanosheets with a thickness of approximately 80 nm. These bilayered nanosheets possess good adhesion to surfaces with complex topography and thus achieve better wound closure than other bulk two-dimensional materials. Moreover, this AMP-grafted conjugation shows minimal cytotoxicity compared with Ag⁺ antibacterial agents, and the antibacterial rate of nanosheets is dependent on the graft rate of AMP. We suggest that this bilayered antibacterial nanosheet might be an advanced anti-infection dressing for wound treatment in clinical settings.

Keywords Nanosheet · Adhesive · Complicated topography · Antimicrobial

Introduction

Bacterial infection is the main cause of wound aggravation and can even lead to severe sepsis [1, 2]. To date, debridement, irrigation-suction and subsequent antibacterial agents

or dressing treatments are effective methods in clinical settings [3, 4]. However, general antibacterial agents, such as antibiotics and Ag⁺ dressings, lead to superbugs or ion-deposition-induced cytotoxicity [5, 6]. Moreover, existing two-dimensional antibacterial dressings, such as antibiotic paste, antibacterial hydrogel and antibacterial films, are usually limited by poor adhesion to surface wounds with complex topography, for instance, diabetic feet, joints and irregular defected tissue, etc. [7–9].

Differing from general two-dimensional materials, films with a nanoscale thickness (i.e. less than 100 nm) possess excellent flexibility, which leads to firm adhesion to any kind of surfaces through only non-covalent adhesion [10]. For example, Toshinori Fujie et al. developed polysaccharide nanosheets and found that the thinner film shows better adhesion. Moreover, to balance the mechanical strength and adhesion, the authors found that the best thickness for the nanosheets was approximately 75 nm. These flexible and adhesive nanosheets were subsequently used in the repairing of tissue defects, wound infection prevention, the controlled release of drugs, as an anti-adhesion barrier, etc. However,

Electronic supplementary material The online version of this article (<https://doi.org/10.1007/s42242-020-00091-7>) contains supplementary material, which is available to authorized users.

✉ Xuetao Shi
shxt@scut.edu.cn

- ¹ Peking University Shenzhen Institute, Peking University, Shenzhen, People's Republic of China
- ² School of Materials Science and Engineering, South China University of Technology, Guangzhou 510640, People's Republic of China
- ³ National Engineering Research Center for Tissue Restoration and Reconstruction, South China University of Technology, Guangzhou 510006, People's Republic of China
- ⁴ Guangzhou Regenerative Medicine and Health Guangdong Laboratory, Guangzhou 510005, People's Republic of China

their antibacterial methods were limited to traditional antimicrobial agents, such as antibiotics or Ag^+ , which might lead to superbugs or ion-deposition-induced cytotoxicity [10–15].

Antimicrobial peptides (AMPs), which can kill bacteria by destroying their cell membrane and which show broad spectrum, high efficiency, and non-bacterial resistance, are thought to be a new antibacterial strategy [16–18]. Moreover, AMPs are easily modified to polymer chains and metal or metalloid inorganic implant scaffolds through EDC/NHS coupling chemistry, click chemistry, double bond polymerization, etc., enhancing their antibacterial property [19–21].

In this report, we proposed the creation of bilayered antibacterial nanosheets by the decoration of thiolated APM onto biocompatible methacrylated gelatine (GelMA) with multiple modification sites by ene-thioalcohol click chemistry and then combining it with biodegraded, high strength, hydrophobic poly-L-lactide (PLLA). The inner antibacterial layer, as well as the outer mechanical layer with different thicknesses, was confirmed to balance the mechanical strength and adhesion of the nanosheets, whereas different amounts of AMP were decorated onto a GelMA side chain to refine their antibacterial property. The surface and interfacial properties and the cytotoxicity were also characterized to confirm the biocompatibility of the bilayered nanosheets.

Materials and methods

Materials

Poly-L-lactide (PLLA, $M_w \sim 300,000$), phosphate-buffered saline (PBS, $\text{pH} = 7.4$), dimethylacetamide (DMAC), 2,6-dimesitylphenylphosphine (DMPPh), sulfadiazine silver (AgSD), polyvinyl alcohol (PVA, $M_w \sim 130,000$) and photoinitiator I2959 were purchased from Sigma-Aldrich, Inc. Dialysis membranes (molecular weight cutoff (MWCO) of 2000 Da) were purchased from Yuanye Biotech, Inc. (Shanghai, China). Antimicrobial peptide (AMP) (KRW-KKWRRRC) and FITC-marked antimicrobial peptide (FITC-Acp-KRWWKWRRC) were purchased from Shanghai Qiangyao Biotechnology Co., Ltd. Silicon wafers were purchased from Lijing Silicon Material Co., Ltd. (Zhejiang, China). Agar and nutrient bouillon were purchased from Shanghai Aladdin Biochemical Technology Co., Ltd. (Shanghai, China). Dulbecco's modified Eagle's medium (DMEM), penicillin, streptomycin, calcein AM, ethidium homodimer and foetal bovine serum (FBS) were obtained from Gibco Company (USA). Cell Counting Kit-8 was purchased from DOJINDO (Japan). Gelatine methacryloyl (GelMA) was prepared according to our previous report (with a substitution degree of $\sim 90\%$) [22], and deionized

(DI) water was used in all experiments. All other chemicals are of analytical grade and used as received.

Synthesis and characterization of GelMA-AMP

The GelMA-AMP conjugates (termed GP) were synthesized using a thiol-ene click chemical reaction. Briefly, GelMA (1.0 g) was dissolved in 10 ml DI water at 25°C in a flask with nitrogen purging. Subsequently, 12.5, 25.0 and 50.0 mg AMP mixed with 2 mg DMPPh was dissolved in 4 ml DMAC and then added to the GelMA solution. After a 1-h reaction, the product was dialysed in DI water for 3 days and then lyophilized. The chemical structure of the product was analysed by normal Hydrogen Nuclear Magnetic Spectrum (HNMR) using D_2O as a solution. For the synthesis of the FITC-marked GP, all of the procedures were consistent with those used in the synthesis of GP, except that APM was replaced by FITC-marked AMP and that the whole process was protected from light to prevent photobleaching of the fluorophore. The solution of FITC-marked GP was packed in capillary tubes with a diameter of 0.26 mm and then observed by confocal laser scanning microscopy (CLSM) (Leica TCS SP-8, Germany); the images obtained were further analysed by ImageJ software.

For the quantitative analysis of the AMP content in GP conjugates, their absorption intensities were tested using UV-vis spectroscopy (Thermo Scientific Nanodrop 2000c, USA). A standard calibration curve was obtained by plotting the absorbance values of characteristic peaks of AMP versus concentrations ranging from 1 to 20 $\mu\text{g/ml}$. The conjugates were dialysed for 3 days at 4°C , after which the dialysate containing free AMP was collected and tested. The conjugation efficiency was then obtained by calculating the quantitative difference between the total amount and free amount of AMP according to the following calculation, where $W\%$ refers to the success rate of the grafting, m_0 refers to the addition of AMP, and c_d and V_d refer to the concentration of AMP in the dialysate solution and the total volume of dialysate solution, respectively.

$$W\% = (m_0 - c_d V_d) / m_0$$

Preparation of freestanding bilayered nanosheets

The nanosheets were fabricated by spin coating [10]. The GP conjugates (75 mg/ml) were mixed with I2959 (1.0% w/v) in an aqueous solution. PVA (30% w/v) solutions were prepared using DI water. PLLA (15 mg/ml) was prepared using dichloromethane. The nanosheets were prepared through the following steps: (1) an aqueous solution of PVA (1 ml) was dropped onto a silicon wafer substrate, after which the substrate was rotated at 2000 rpm for 30 s and then dried in

air. (2) PLLA solution (1 ml) was dropped onto the PVA layer to build the second layer, and the substrate was rotated at 6000 rpm for 20 s and dried by N₂ flow. (3) The PLLA layer was treated with plasma (100% O₂, gas input time of 120 s, processing time of 10 min). (4) GP solution (1 ml) was dropped onto the PLLA layer, and then the silicon wafer was rotated at 6000 rpm for 20 s and dried by N₂ flow. (5) The GP layer was then crosslinked under UV irradiation (5 mW/cm²) for 10 min. (6) The GP/PLLA nanosheets, along with the PVA layer, were able to be peeled off from the silicon wafer substrate using tweezers and subsequently used for wound repair. The nanosheets were photographed using a digital camera (PowerShot G5X, Cannon Co., Japan), and the thicknesses of samples were analysed by a surface profiler (WykoNT1100-Veeco Corp., USA). Static water contact angles of PLLA, plasma-treated PLLA and GP coated on silicon wafers were measured by a contact angle measurement instrument (KRUSS DSA25, Germany) after placing 20 µl of water onto the sample surfaces for 10 s.

The PVA-supported film was immersed in water. After the bilayered nanosheets were released from water by the dissolution of PVA layer, the nanosheets were dredged up from water by plastic plate and used for observing the morphology of cross section by field-emission scanning electron microscopy (FE-SEM) (MERLIN, Carl Zeiss AG, Germany) at an accelerating voltage of 5 kV. The overall morphologies were assessed by scanning electron microscopy (SEM) observation of the bilayered nanosheets with an SEM at an accelerating voltage of 15 kV after the samples were placed onto the conductive adhesive and then coated with platinum (~5 nm thickness). The surface roughness of the nanosheets was also characterized by an atomic force microscope (AFM) (MFP-3D-S, Asylum Research, USA) under tapping mode with a 0.8 n/m probe.

For the preparation of AgSD-loaded antibacterial nanosheets, all of the methods were consistent with those used for the fabrication of GP/PLLA nanosheets except that GP solution was replaced by the GelMA solution mixed with 4, 8 and 16 mg/ml of AgSD.

Adhesive performance of nanosheets

The adhesive properties of nanosheets were also evaluated by applying them to porcine muscle. The prepared freestanding film was peeled off from the silicon wafer substrate and then pasted to porcine tissue, and after the dissolution of the PVA support layer using DI water, the bilayered nanosheets were released from the freestanding film and applied to the tissue. The nanosheet-pasted tissue was then stretched, compressed, and twisted by tweezers, and all of the processes were recorded by a digital camera (PowerShot G5X, Cannon Co., Japan).

To compare the adhesive behaviours between nanosheets and another bulk dressing, the Band-Aid, a general film with a thickness in micron scale and nanosheets were also applied to complicated surfaces such as human joints, and their adhesive performances were observed and recorded by digital camera.

To evaluate the adhesive performance of the bilayered nanosheets under wet conditions, the nanosheets were pasted onto a porcine skin and then immersed into water. The adhesive performance of the nanosheets was observed and recorded by a digital camera every day.

We also performed a quantitative analysis on the adhesive performance of the nanosheets by micro scratch test. Firstly, we fabricated nanosheets with a thickness of ~80 nm (prepared by using 75 mg/ml of GP and 15 mg/ml of PLLA) and ~390 nm (prepared by using 75 mg/ml of GP and 40 mg/ml of PLLA). Subsequently, the bilayered nanosheets were pasted to a 2 × 2 cm glass substrate. Then, the diamond stylus of the micro scratch tester oscillated parallel to the surface of the nanosheets until the film was scarified. The critical loading was recorded as the adhesive strength of the nanosheets.

Antibacterial performance of nanosheets

The nanosheets used here were fabricated on silicon wafers with 14 mm diameter using the same technology we had mentioned before. The antimicrobial activities of the nanosheets were evaluated by co-culturing them with *E. coli* and *S. aureus* in plates. Prior to bacterial seeding, each of the 24-well plates with nanosheets was sterilized with 75% ethanol for 0.5 h and then washed three times with sterile PBS. 200 µl of the bacterial suspension with the concentration at 1×10^7 CFU/ml was added to each well to inundate the surface of the samples. The samples were cultured at 37 °C for 8 h. After gradient dilution using PBS, 10 µl of a bacterial suspension of each sample was extracted and then spread on the agar plate until the medium was solidified. The plate coated with a bacterial suspension was cultured overnight at 37 °C, and the antibacterial activity was evaluated by calculating the number of bacterial colonies.

Cytotoxicity studies

The nanosheets used here were fabricated on silicon wafers with 14 mm diameter using the same technology we had mentioned before. Mouse embryonic fibroblasts (MEFs) were acquired from Cyagen Biosciences. The cells were cultured in DMEM with 10% of FBS and 100 U/100 mg of penicillin/streptomycin (Invitrogen) and were kept in an incubator under standard environment. To evaluate the cytotoxicity of the nanosheets, MEFs (10,000 per well) were implanted in normal medium in a 24-well plate with

glass substrates coated with nanosheets made of GelMA mixture with different AgSD or GP with contents with a range of AMP content. The well without nanosheets served as a control group. After being cultured for 24 h, the cells were rinsed twice with PBS. Then, the MEFs were incubated in 200 μ l live/dead staining kit (1.5 μ l of calcein AM and 0.5 μ l of ethidium homodimer mixed in 1 ml of PBS) at 25 °C for 45 min. After the staining solution was removed, each well was washed three times with PBS and observed using an inverted fluorescence microscope (Eclipse TieU, Nikon, Japan). The live cells were stained green and the dead cells were dyed red. Cell viability was assessed using a cell counting kit-8 (CCK-8, Dojindo Laboratories, USA). Briefly, the MEFs were cultivated in a 48-well plate at a density of 5000 per well in the presence of glass substrates coated with nanosheet samples. The well without nanosheets served as a control group. After culturing for 1, 3 and 5 days, the cells in the 48-well plate were immersed in 300 μ l of CCK-8 solution and cultured at 37 °C for 1 h at regular intervals. Then, 100 μ l of the incubated medium was extracted to a 96-well plate and wrapped in tin foil to protect it from fluorescence quenching. The absorbance at 450 nm of the samples was recorded using a multifunctional microplate reader (Thermo 3001, ThermoFisher Scientific, USA).

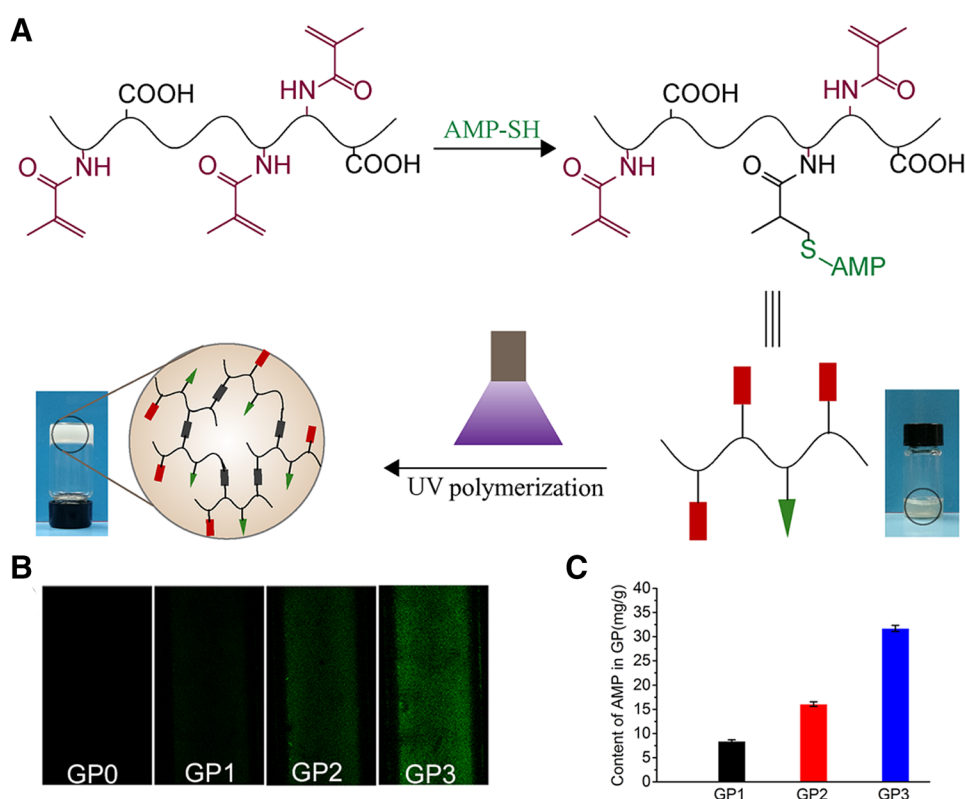
Results and discussions

Synthesis and characterization of GelMA-AMP

Figure 1a shows the synthesis diagram of the GP conjugate. We chose GelMA as a substrate because of its good biocompatibility, multiple functional groups that could be modified in several ways, and because it is curable under mild conditions [23–25]. However, GelMA does not have any antibacterial inherent properties. Herein, sulfhydryl-groups-contained antimicrobial peptides (SH-KRWWKWRRRC) were modified onto the GelMA using a thiol-ene click chemical reaction. Only trace amounts of AMP that induced to GelMA can endow it with good antibacterial capability due to the highly efficient antimicrobial properties of AMP. Hence, the consumption of ene groups of GelMA by the thiol groups of AMP was little. As a result, the GP conjugate was still UV-curable.

Since the amount of AMP that we added to GelMA was very small, the content of APM in GD was also tiny. Because both of them share common characteristic functional groups, such as amides and carboxyls, it was difficult to characterize the structural differences between GelMA and GelMA-AMP using common techniques (for example, HNMR, as we can see in Figure S1). The fluorescence labelling method sheds new light on GelMA and GelMA-AMP [26]. Herein,

Fig. 1 Synthesis and characterization of AMP-grafted GelMA. **a** Synthetic schematic diagram of GP conjugate and subsequent UV cross-linking that initiated double bond polymerization. **b** Fluorescence images of FITC-marked GP with different grafted amounts of AMP. **c** Amounts of grafted AMP in GP1, GP2 and GP3



different amounts of FITC-marked AMP, varying between 0, 12.5, 25 and 50 mg/g, were chosen to react with GelMA, and their fluorescence was characterized by confocal laser scanning microscopy. As we can see in Fig. 1b, with increasing of amounts of FITC-marked AMP added to the reaction system, the fluorescence intensity was enhanced. This phenomenon strongly proved the APM had been grafted to the GelMA skeleton successfully. To further confirm the amount of grafted AMP, the conjugates were dialysed for 3 days at 4 °C, after which the dialysate containing free AMP was collected and tested using UV–vis. The conjugation efficiency was then obtained by calculating the quantitative difference between the total amount and the free amount of AMP. According to the UV–vis curves in Figure S2 and the standard AMP curve (inset) associated with the above calculation, we suggest that the amounts of grafted AMP in GP1, GP2 and GP3 were 8.4 mg/g, 16.1 mg/g and 31.7 mg/g, respectively (Fig. 1c). These data suggested that we successfully constructed a series of GelMA-AMP with different amounts of AMP.

Preparation of freestanding bilayered nanosheets

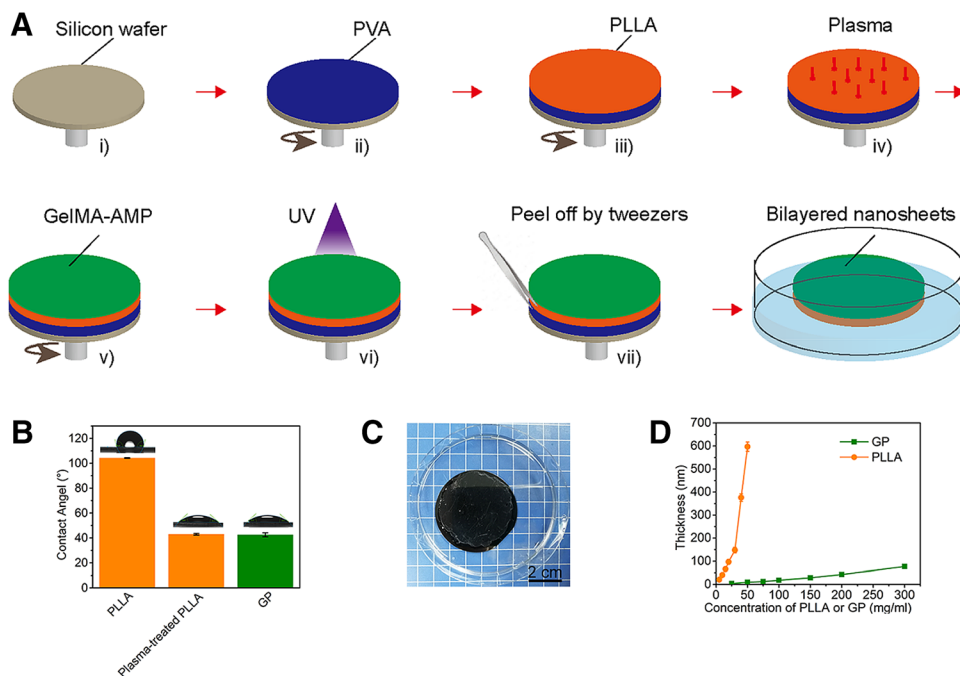
We fabricated the bilayered nanosheets by spin coating (Fig. 2a). Since the flexible nanosheets are easily wrinkled without any substrates, hydrosoluble PVA was chosen as a “supporting layer” or “sacrifice layer”, which could be removed by rinsing and hence made the nanosheets easy to manipulate. After that, hydrophobic PLLA was induced as the out mechanical layer of the nanosheet. However, this structural design also led to another issue: it was also

difficult to achieve a good combination between the hydrophobic PLLA layer and hydrophilic GP layer. Here, plasma treatment that endows an object with hydrophilic properties was introduced before the deposition of the antibacterial GP [27, 28]. As we can see in Fig. 2b, before plasma, the water contact angles of PLLA are $104.2 \pm 0.28^\circ$ without plasma treatment and $42.9 \pm 0.66^\circ$ with plasma treatment. The latter one is very close to the contact angle of GP ($42.5 \pm 1.56^\circ$). After the preparation of the GP layer and solidification by UV light, the bilayered nanosheets supported by the PVA layer could be peeled off by tweezers. This film was subsequently immersed into water, and finally, the GP/PLLA bilayered nanosheets were released (Fig. 2c).

The adhesive property of nanosheets is related to their thickness, and it was proven that nanosheets with a thickness of approximately 75 nm achieved good adhesion, as well as good mechanical strength [10]. To balance these, different concentrations of GP and PLLA were used to prepare the nanosheets, and their thicknesses were tested by surface profiler (Fig. 2d). Finally, we chose 15 mg/ml of PLLA and 75 mg/ml GP, with a total thickness of 80.2 ± 8.67 nm, which is very close to previous studies and might meet our demands in wound repairing. We also observed the morphology of cross section of nanosheets by FE-SEM. After the bilayered nanosheets were released from water, it was dredged up from the water by plastic plate (Fig. 3a) and used for observing the morphology of cross section of nanosheets. As we can see in Fig. 3b, the thickness of the nanosheets was about ~80 nm.

To better understand the surface topography of the nanosheets, SEM and AFM measurements were also

Fig. 2 Preparation of nanosheets. **a** Fabrication process of nanosheets by spin coating. **b** Static contact angle of nanosheets. **c** GP/PLLA bilayered nanosheets released from silicon substrate in an aqueous solution. **d** Thickness of the PLLA layer and GP layer at different concentrations



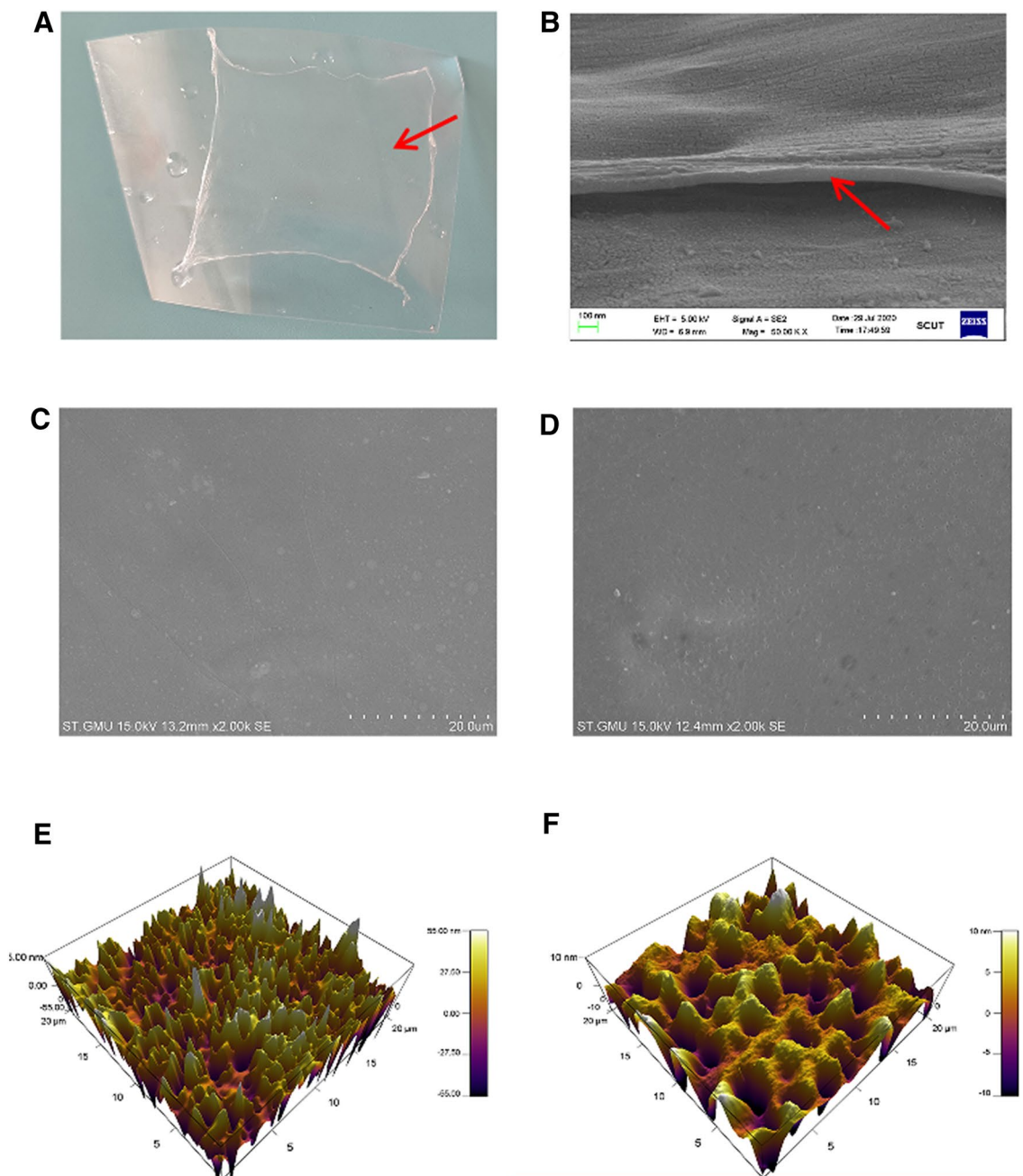


Fig. 3 Topography characterization of nanosheets. **a** Nanosheets were dredged up from water by plastic plate and used for observing, **b** the morphology of cross section of nanosheets. The nanosheets were

marked by arrows. **c** SEM morphology of PLLA (~ 70 nm) and **d** GP/PLLA (~ 80 nm) bilayered nanosheet. **e** AFM morphology of PLLA and **f** GP/PLLA bilayered nanosheet

conducted. As we can see in Fig. 3c–f, the surface topography of the PLLA layer is very smooth. After the introduction of the GP layer, the surface roughness of the nanosheets decreases to some extent (from ~ 28.6 to ~ 5.0 nm). However, the change in the surface roughness is still very limited in overall scope. These data suggest that we had succeeded in the construction of a GP/PLLA bilayered nanosheets by spin coating.

Adhesive performance of nanosheets

To prevent wounds from infection, extrinsic sources of infection should be prevented from contacting the wound. That is, the wound should be closed at first [29]. However, the surface topographies of a wound are usually complicated, and general two-dimensional materials such as Band-Aids and general films showed poor adhesion to complicated surfaces

(for example, joints) and resulted in the failure of the wound closure because of their lack of flexibility (Fig. 4a). The developments in nanotechnology led to the successful construction of nanosheets with a large aspect ratio. These nanosheets are highly flexible and hence can adhere to complicated surfaces by non-covalent adhesion without any adhesive agents and finally achieve wound closure (Fig. 4a). Considering that wounds are suffered from external stress in people's daily life, the adhesive performance of nanosheets to the tissue under stress conditions were also tested. As we can see in Fig. 4b, after the PVA supporting layer was removed by water, the nanosheets adhered to the surface of porcine muscle at first. By applying external stress, such as stretching, compression and twisting using tweezers, the nanosheets still firmly adhered to the tissue.

Most of the wounds are in wet conditions because of the exudation of tissue fluids. As a dressing, whether the nanosheets can keep adhesive under a wet environment is very important. Herein, the adhesive performance of nanosheets under a wet environment was evaluated by pasting the nanosheets to porcine tissue and immersed into water for a period of time. As we can see in Fig. 4c, the bilayered nanosheets kept adhesive under water for more than 3 days.

We also performed a quantitative analysis on the adhesive performance of the nanosheets by a micro scratch

test (Figure S3A). The point at which adhesive failure occurs (“critical load”) reflects the adhesive strength of the nanosheets. As we can see in Figure S3B and C, the adhesive strength of the nanosheets was related to the thickness of the film. Moreover, nanosheets with thickness less than 100 nm showed high adhesive strength than thick films. These data suggest that we had constructed bilayered nanosheets with high flexibility and good adhesion to a surface with complex topography.

Antibacterial performance and cytotoxicity studies of nanosheets

Differing from general antimicrobial agents, the AMPs kill bacteria by destroying their cytomembrane and show broad spectrum, high efficiency and no bacterial resistance to its antimicrobial properties. To confirm whether the AMP maintains its high efficiency when grafted to the polymer chain, the antibacterial rates of different concentrations of AMP in GP named GD1 (0.63 mg/ml), GD2 (1.2 mg/ml) and GD3 (2.4 mg/ml) were tested. Meanwhile, Ag⁺-loaded GelMA nanosheets with different AgSD contents (4, 8, and 16 mg/ml) were also measured in order to compare the efficiency of the two antibacterial agents. As we can see in Fig. 5a–d, both of the Ag⁺-loaded GelMA and GP samples

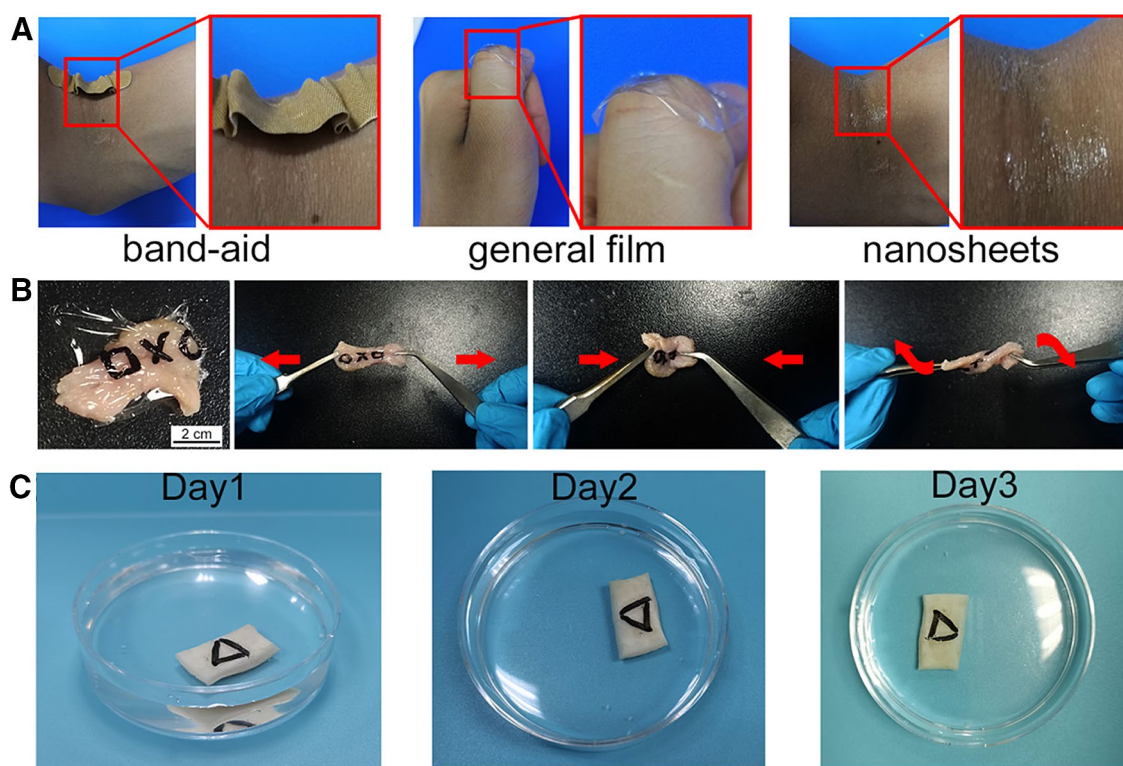
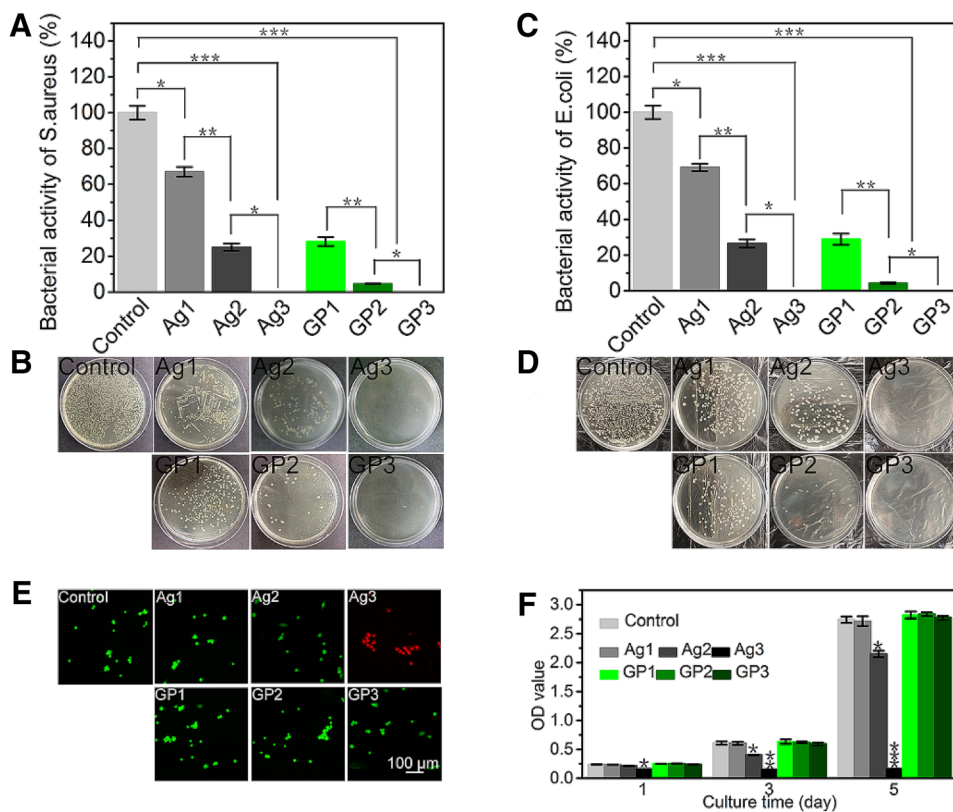


Fig. 4 Adhesive performance of the nanosheets. **a** Adhesive performance of a Band-Aid, general film and nanosheets to surface with complex morphology. **b** Adhesive performance of nanosheets to porcine muscle when suffering from stretching, compressing and twisting. **c** Adhesive performance of nanosheets to porcine tissue under water in 3 days

test (Figure S3A). The point at which adhesive failure occurs (“critical load”) reflects the adhesive strength of the nanosheets. As we can see in Figure S3B and C, the adhesive strength of the nanosheets was related to the thickness of the film. Moreover, nanosheets with thickness less than 100 nm showed high adhesive strength than thick films. These data suggest that we had constructed bilayered nanosheets with high flexibility and good adhesion to a surface with complex topography.

Fig. 5 Antibacterial performances and biocompatibilities of nanosheets with different kinds and amounts of antibacterial agents. **a** Bacterial viability of *S. aureus* after culturing for 24 h with samples and **b** the corresponding bacterial colony images. **c** Bacterial viability of *E. coli* after culturing for 24 h with samples and **d** the corresponding bacterial colony images. **e** Live/dead fluorescence images of MEFs after culturing on nanosheets for 1 day. A normal complete medium served as the control group. The live cells were stained green and the dead cells were stained red. **f** Cell viability of MEFs after culturing on nanosheets for 1, 3 and 5 days. Data are displayed as the mean \pm standard error ($n=3$). (* $p < 0.05$, ** $p < 0.01$, *** $p < 0.001$.)



show good antimicrobial properties to gram-negative bacteria and gram-positive bacteria with close bacterial viability. Moreover, the GP groups show better efficiency than Ag^+ samples because the content of AMP in all samples was lower than that of the Ag^+ -contained samples. When comparing samples with a bacterial viability rate of $\sim 30\%$, we calculated that the antibacterial efficiency of GP was almost 13 times than that of the AgSD-loaded GelMA. To achieve more than a 100% antibacterial rate, the content of AgSD should reach 16 mg/ml; meanwhile, the AMP content of GP for a similar rate was 2.4 mg/ml.

We subsequently evaluated the biocompatibilities of AgSD-load GelMA nanosheets and GP nanosheets by coculturing the MEFs cell with different samples. After 24 h of culturing, the live/dead staining was conducted in all samples. The results in Fig. 5e, f show that all of the samples except the Ag3 sample showed minor cytotoxicity in the short term. Moreover, when we further evaluated the cell proliferation of the nanosheet samples by CCK8 analysis, we found that the Ag3 group showed serious cytotoxicity over the whole period of time with the lowest OD value. Furthermore, on the 3rd and 5th day, the OD value of the Ag2 group was also lower than that of the control group, which meant that it showed certain cytotoxicity in long term. In contrast, the GP groups showed good long-term biocompatibilities. All of these data proved that the

GP is a safer and more efficient method than Ag^+ -loaded materials in antibacterial wound treatment.

Conclusion

In summary, we have succeeded in the construction of bilayered antimicrobial nanosheets through spin coating. The AMP-modified GP conjugate was synthesized and served as an antibacterial layer to kill the endogenous infection; meanwhile, PLLA was introduced due to its good mechanical property. Compared to general antibacterial agents such as Ag^+ , the GP nanosheets showed higher antibacterial efficiency as well as good biocompatibility. Moreover, due to the inherent flexibility, these antimicrobial bilayered nanosheets firmly adhered to surfaces with complicated morphology and thereby achieved complex wound closure. These bilayered nanosheets might be an advanced antibacterial dressing and could be used for preventing complicated wounds from infection in clinical.

Acknowledgements We would like to thank the Shenzhen Science and Technology Program (JCYJ20170815153105076, GJHZ20180411143347603), the Guangdong Natural Science Funds for Distinguished Young Scholars (2016A030306018), the Science and Technology Program of Guangdong Province (2019B010941002, 2017B090911008), Outstanding Scholar Program

of Guangzhou Regenerative Medicine and Health Guangdong Laboratory (2018GZR110102001), the National Nature Science Foundation of China (Grants U1801252) and the Science and Technology Program of Guangzhou (201804020060), the Science and Technology Program of Guangzhou (201804020060, 202007020002).

Author Contributions Chengkai Xuan participated in the experimental research, data analysis, writing and editing of the manuscript. Xuemin Liu and Chen Lai performed the data analysis and the editing of the manuscript. Xuetao Shi performed the study design and editing of the manuscript. All authors have read and approved the final manuscript and, therefore, have full access to all the data in the study and take responsibility for the integrity and security of the data.

Data availability The data used and analysed during the current study are available from the corresponding author on reasonable request.

Compliance with ethical standards

Conflict of interest The authors declare that there is no conflict of interest.

Ethics approval This article does not contain any studies with human or animal subjects performed by any of the authors.

References

1. Marsh CB, Wewers MD (1996) The pathogenesis of sepsis: factors that modulate the response to gram-negative bacterial infection. *Clin Chest Med* 17:183–197. [https://doi.org/10.1016/S0272-5231\(05\)70308-7](https://doi.org/10.1016/S0272-5231(05)70308-7)
2. Gottrup F (2004) A specialized wound-healing center concept: importance of a multidisciplinary department structure and surgical treatment facilities in the treatment of chronic wounds. *Am J Surg* 187:S38–S43. [https://doi.org/10.1016/S0002-9610\(03\)00303-9](https://doi.org/10.1016/S0002-9610(03)00303-9)
3. Campoccia Davide, Montanaro Lucio, Arciola Carla Renata (2013) A review of the clinical implications of anti-infective biomaterials and infection-resistant surfaces. *Biomaterials* 34:8018–8029. <https://doi.org/10.1016/j.biomaterials.2013.07.048>
4. Deery HG II (1998) Outpatient parenteral anti-infective therapy for skin and soft-tissue infections. *Infect Dis Clin North Am* 12:935–949. [https://doi.org/10.1016/S0891-5520\(05\)70029-5](https://doi.org/10.1016/S0891-5520(05)70029-5)
5. Yao JD, Moellering RC (2011) Antibacterial agents, manual of clinical microbiology, 10th edn. American Society of Microbiology, Washington, DC, pp 1043–1081
6. Davies D (2003) Understanding biofilm resistance to antibacterial agents. *Nat Rev Drug Discov* 2:114–122. <https://doi.org/10.1038/nrd1008>
7. Luo Y, Zhao R, Pendry JB (2014) Van der Waals interactions at the nanoscale: the effects of nonlocality. *Proc Natl Acad Sci* 111:18422–18427. <https://doi.org/10.1073/pnas.1420551111>
8. Parsegian VA (2005) Van der Waals forces: a handbook for biologists, chemists, engineers, and physicists. Cambridge University, London
9. Novoselov KS, Mishchenko A, Carvalho A, Neto AC (2016) 2D materials and van der Waals heterostructures. *Science* 353:9439. <https://doi.org/10.1126/science.aac9439>
10. Fujie T, Matsutani N, Kinoshita M, Okamura Y, Saito A, Takeoka S (2009) Adhesive, flexible, and robust polysaccharide nanosheets integrated for tissue-defect repair. *Adv Func Mater* 19:2560–2568. <https://doi.org/10.1002/adfm.200900103>
11. Fujie T, Ahadian S, Liu H, Chang H, Ostrovidov S, Wu H, Khademhosseini A (2013) Engineered nanomembranes for directing cellular organization toward flexible biodevices. *Nano Lett* 13:3185–3192. <https://doi.org/10.1021/nl401237s>
12. Niwa D, Koide M, Fujie T, Goda N, Takeoka S (2013) Application of nanosheets as an anti-adhesion barrier in partial hepatectomy. *J Biomed Mater Res B Appl Biomater* 101:1251–1258. <https://doi.org/10.1002/jbm.b.32937>
13. Ricotti L, Taccola S, Pensabene V, Mattoli V, Fujie T, Takeoka S, Dario P (2010) Adhesion and proliferation of skeletal muscle cells on single layer poly (lactic acid) ultra-thin films. *Biomed Microdevice* 12:809–819. <https://doi.org/10.1007/s10544-010-9435-0>
14. Fujie T, Ricotti L, Desii A, Menciassi A, Dario P, Mattoli V (2011) Evaluation of substrata effect on cell adhesion properties using freestanding poly (l-lactic acid) nanosheets. *Langmuir* 27:13173–13182. <https://doi.org/10.1021/la203140a>
15. Miyazaki H, Kinoshita M, Saito A, Fujie T, Kabata K, Hara E, Saitoh D (2012) An ultrathin poly (l-lactic acid) nanosheet as a burn wound dressing for protection against bacterial infection. *Wound Repair Regen* 20:573–579. <https://doi.org/10.1111/j.1524-475X.2012.00811.x>
16. Reddy KVR, Yedery RD, Aranha C (2004) Antimicrobial peptides: premises and promises. *Int J Antimicrob Agents* 24:536–547. <https://doi.org/10.1016/j.ijantimicag.2004.09.005>
17. Fjell CD, Hiss JA, Hancock RE, Schneider G (2012) Designing antimicrobial peptides: form follows function. *Nat Rev Drug Discov* 11:37–51. <https://doi.org/10.1038/nrd3591>
18. Koczulla AR, Bals R (2003) Antimicrobial peptides. *Drugs* 63(4):389–406. <https://doi.org/10.2165/00003495-200363040-00005>
19. Silva RR, Avelino KYPS, Ribeiro KL, Franco OL, Oliveira MD, Andrade CA (2016) Chemical immobilization of antimicrobial peptides on biomaterial surfaces. *Front Biosci (Schol Ed)* 8:129–142. <https://doi.org/10.2741/s453>
20. Cleophas RT, Riool M, Quarles van Ufford HLC, Zaat SA, Kruijtzter JA, Liskamp RM (2014) Convenient preparation of bactericidal hydrogels by covalent attachment of stabilized antimicrobial peptides using thiol–ene click chemistry. *ACS Macro Lett* 3:477–480. <https://doi.org/10.1021/mz5001465>
21. He J, Chen J, Hu G, Wang L, Zheng J, Zhan J, Wang Y (2018) Immobilization of an antimicrobial peptide on silicon surface with stable activity by click chemistry. *J Mater Chem B* 6:68–74. <https://doi.org/10.1039/C7TB02557B>
22. Liu L, Li X, Shi X, Wang Y (2018) Injectable alendronate-functionalized GelMA hydrogels for mineralization and osteogenesis. *RSC Adv* 8:22764–22776. <https://doi.org/10.1039/C8RA03550D>
23. Mahadik BP, Haba SP, Skertich LJ, Harley BA (2015) The use of covalently immobilized stem cell factor to selectively affect hematopoietic stem cell activity within a gelatin hydrogel. *Biomaterials* 67:297–307. <https://doi.org/10.1016/j.biomaterials.2015.07.042>
24. Nichol JW, Koshy ST, Bae H, Hwang CM, Yamanlar S, Khademhosseini A (2010) Cell-laden microengineered gelatin methacrylate hydrogels. *Biomaterials* 31:5536–5544. <https://doi.org/10.1016/j.biomaterials.2010.03.064>
25. Fang X, Xie J, Zhong L, Li J, Rong D, Li X, Ouyang J (2016) Biomimetic gelatin methacrylamide hydrogel scaffolds for bone tissue engineering. *J Mater Chem B* 4:1070–1080. <https://doi.org/10.1039/C5TB02251G>
26. Lacroix M, Poinso V, Fournier C, Couderc F (2005) Laser-induced fluorescence detection schemes for the analysis of proteins and peptides using capillary electrophoresis. *Electrophoresis* 26:2608–2621. <https://doi.org/10.1002/elps.200410414>
27. Okabe Y, Kurihara S, Yajima T, Seki Y, Nakamura I, Takano I (2005) Formation of super-hydrophilic surface of hydroxyapatite

- by ion implantation and plasma treatment. *Surf Coat Technol* 196:303–306. <https://doi.org/10.1016/j.surfcoat.2004.08.190>
28. Han JB, Wang X, Wang N, Wei ZH, Yu GP, Zhou ZG, Wang QQ (2006) Effect of plasma treatment on hydrophilic properties of TiO₂ thin films. *Surf Coat Technol* 200(16–17):4876–4878
29. Zelko JR, Moore EE (1981) Primary closure of the contaminated wound: closed suction wound catheter. *Am J Surg* 142:704–706. [https://doi.org/10.1016/0002-9610\(81\)90316-0](https://doi.org/10.1016/0002-9610(81)90316-0)